Chapter 4

A Regularised Solution to the Bridge-Weigh-In-Motion Equations

4.1 Introduction

This chapter proposes a new method to identify the static axle and gross vehicle weights of trucks as they traverse a bridge. The method is an extension of the Bridge Weigh in Motion (B-WIM) algorithm introduced by Moses (1979) and developed by Peters (1984, 1986), O'Brien (1999a) and Znidaric (1998). The method of regularisation is applied to the B-WIM algorithm to improve the errors that are generally encountered in calculated static axle weights. The algorithm is tested using dynamic simulations from a 1d finite element model of a beam subject to moving constant and time varying forces. Further to this the algorithm is tested using dynamic simulations from an eleven-degree of freedom vehicle bridge interaction model with a random road profile developed by Green (1995).

4.2 Bridge Model and Dynamic Simulation

A 20m simply supported bridge is idealised as a 1 dimensional beam using the finite element method. This bridge model has a cross-section of area (A) 8 m^2 and second moment of Area (I) of 0.667 m^4. Other material properties are Young's modulus (E) of 3.5 x 10^{10} N/m^2 and density (ρ) of 2400 kg/m^3. The beam is discretized into twenty equal elementary beams of length l_e, see figure (4.1), and two degrees of freedom (rotation, θ, and displacement, y) at each end node. For an elementary beam, the elemental stiffness and consistent mass matrices are defined in equations (2.81) and (2.82) and Appendix D. The global stiffness and mass matrices were generated using a program developed in Matlab. The model was validated using an eigenvalue analysis of the natural frequencies in Matlab, and a good match was found between the calculated frequencies from the finite element model in Matlab and the theoretical natural frequencies, see table 4.1.

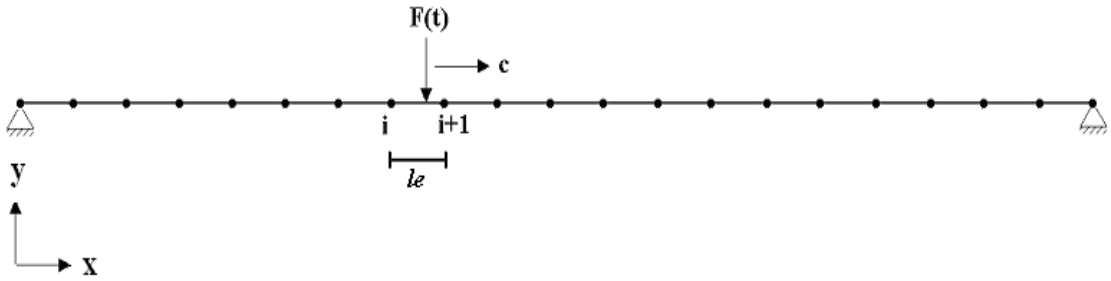

Figure 4.1 - Finite Element model of bridge subject to a moving force F(t)

Mode Number	Theoretical Natural frequency (Hz)	Natural frequency from FE model (Hz)
1	**4.329**	**4.329**
2	**17.316**	**17.317**
3	**38.962**	**38.963**
4	**69.265**	**69.273**
5	**108.230**	**108.26**
6	**155.850**	**155.93**
7	**212.130**	**212.33**
8	**277.060**	**277.52**
9	**350.660**	**351.58**
10	**432.910**	**434.62**

Table 4.1 – Theoretical natural frequencies compared with the natural frequencies form the finite element model

The global stiffness $[K_g]$ and mass matrices $[M_g]$ are of size [42 x 42] corresponding to 21 translations, and 21 rotations for the 21 nodes in the model. With the assumption of zero damping in the model, the equilibrium equation of motion for the bridge subject to a moving force with constant velocity reduces to,

$$[M_g]\{\ddot{y}\} + [K_g]\{y\} = F^e \tag{4.1}$$

where $\{y\}$ is the vector of displacements for all degrees of freedom and $\{F^e\}$ is the elemental force vector. The actual moving load (F^t) is distributed as a product of the hermite shape functions to the degrees of freedom of the i^{th} element that the force is acting on, see figures 4.1 and 4.2. The shape functions for the elementary beam element are defined by,

$$N_1(x) = 1 - \frac{3x^2}{l_e^2} + \frac{2x^3}{l_e^3} \tag{4.2}$$

$$N_2(x) = x - \frac{2x^2}{l_e} + \frac{x^3}{l_e^2} \tag{4.3}$$

$$N_3(x) = \frac{3x^2}{l_e^2} - \frac{2x^3}{l_e^3} \tag{4.4}$$

$$N_4(x) = -\frac{x^2}{l_e} + \frac{x^3}{l_e^2} \tag{4.5}$$

where l_e is the element length that the force is acting on. Now for a force (F^t) acting at a distance x_o from the left hand side of the beam, the elemental load vector can be defined by,

$$F^e = \int_0^{l_e} F^t \delta(x - x_o) \begin{Bmatrix} N_1(x_o) \\ N_2(x_o) \\ N_3(x_o) \\ N_4(x_o) \end{Bmatrix} dx = F^t \begin{Bmatrix} N_1(x_o) \\ N_2(x_o) \\ N_3(x_o) \\ N_4(x_o) \end{Bmatrix} \tag{4.6}$$

In this way the original force (F^t) that was acting between nodes is now replaced with an equivalent system where the force is replaced with two transverse forces and two moments. Consequently for a series of moving forces, each force can be distributed to the degrees of freedom for the particular element that it is acting on, as a product of the shape functions.

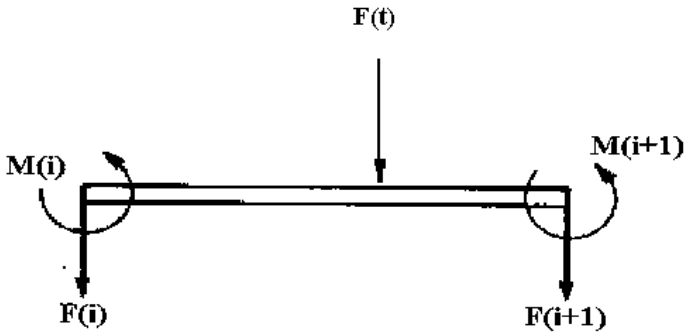

Figure 4.2 - Theoretical force distributed to the elemental degrees of freedom.

With the above definitions the equilibrium equation of motion can be solved using some form of a direct integration scheme. The Newmark Beta direct integration scheme was chosen initially, see Craig (1981), Clough and Penzien (1978) and Appendix E. The equilibrium equation of motion can also be solved using the state space formulation defined in section (2.2.1). The solution to the differential equation defined in equation (2.19) is based on the Pade approximation that,

$$\{f(\tau)\} = \{f(t)\} = \{f_j\} \tag{4.7}$$

over the interval,

$$t \le \tau \le t + h \tag{4.8}$$

such that $f(\tau)$ is approximately equal to $f(t)$. Trujillo (1975) has shown that the approximation to the forcing function of equation (4.7) can replaced by a by a set of piecewise linear segments defined by,

$$\{f(\tau)\} \sim \{f_j\} + \frac{\tau - t}{h}\left\{\{f_{j+1}\} - \{f_j\}\right\} \tag{4.9}$$

over the interval,

$$t \le \tau \le t + h \tag{4.10}$$

where j is the particular time step, h is the sampling time and f is the elemental load vector at each time step. Substituting equation (4.7) into equation (2.22) defined in section (2.2.1), results in a solution defined by,

$$\{X\}_{j+1} = D_1 \{X\}_j + D_2 \{\mathrm{f}\}_{j+1} + D_3 \{\mathrm{f}_j - \mathrm{f}_{j+1}\} \tag{4.11}$$

where,

$$D_1 = e^{Ah} \tag{4.12}$$

$$D_2 = (e^{Ah} - I)[A]^{-1} \tag{4.13}$$

$$D_3 = [e^{Ah} - (e^{Ah} - I)[A]^{-1}][A]^{-1} / h \tag{4.14}$$

Tujillo (1975) states that the advantages of using a formulation of this type are that the system is unconditionally stable with respect to the step size h, and the formulation results in a exact solution for cases where the system matrix [A] is constant or variant with respect to time, where $f(t)$ is truly a piecewise linear function (Trujillo 1975 and Trujillo and Busby 1997). Both the Newmark Beta direct integration scheme and the state space formulation as defined in equation (4.11) were programmed in Matlab. Both models were validated with a P-load moving force model where the closed from solution is given by Fryba (1972). Figure 4.3 shows the midspan displacement of the bridge due to a constant force of 80,000 N travelling at 20 m/s.

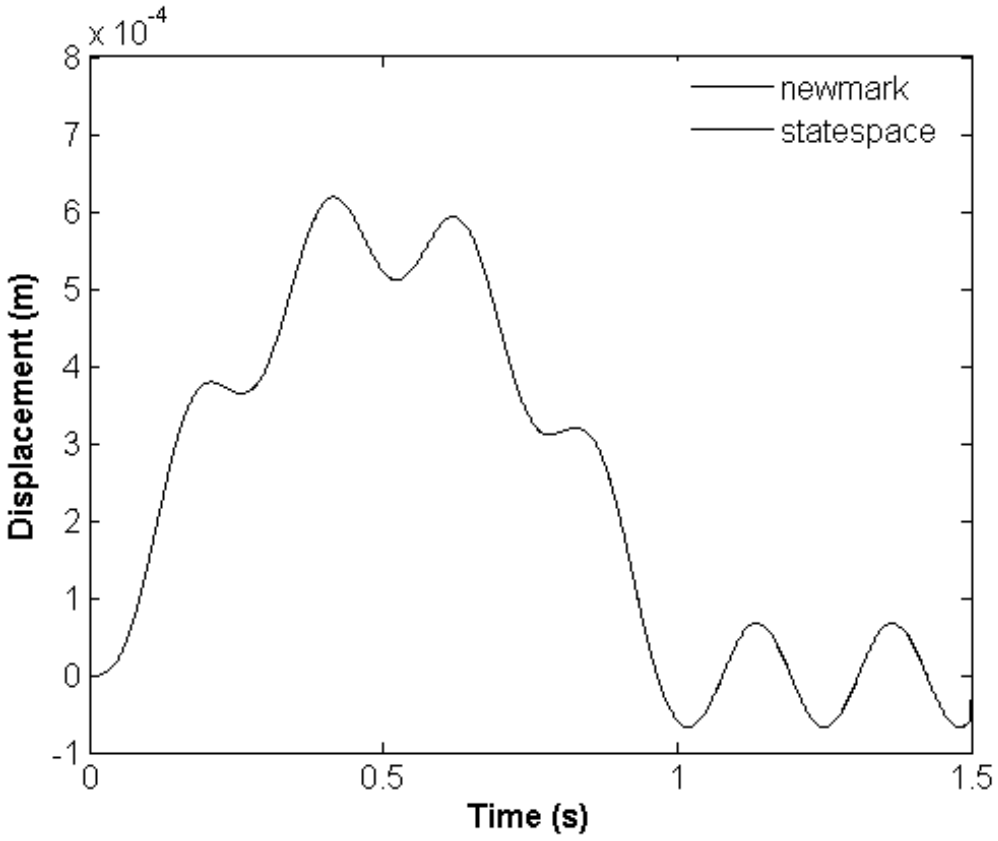

Figure 4.3 – Simulation of a constant moving force using 2 methods of integration

4.3 Regularisation of the Moses Equations

The original Bridge weigh in motion equations were developed by Moses in the 1970's (Moses 1978). The original algorithm was developed for application to the composite beam and slab bridges. The algorithm is based on the concept of static influence lines, whereby the strains or bending moments induced in a structure due to the passage of a moving force are proportional to the product of the static axle weight and the corresponding influence ordinate. In the 1980's, Peters (1984) developed AXWAY in Australia. This B-WIM system is based on the same concept of influence lines. A few years later, he derived a more effective system for weighing trucks using culverts, known as CULWAY (Peters 1986). Both the American and Australian systems have been used for commercial applications on bridges and culverts. Bridge Weighing Systems Inc. developed one of the first commercial B-WIM systems in 1989 on the basis of Moses' algorithm (Snyder 1992). In the 1990's, three new B-WIM systems

were developed independently in Ireland, Slovenia and Japan (O'Brien et al 1999a, Žnidarič & Baumgärtner 1998, Ojio et al. 2000). All of these B-WIM systems use algorithms based on static equations combined with measurements at one single longitudinal section. Many alternative approaches have been discussed in the literature (Leming & Stalford 2002, 2003, Gonzalez et al 2002, Gonzalez 2001) but Moses' algorithm and variations thereon appear to be the basis for commercial B-WIM systems. However, noise, inaccurate assumed shapes for influence lines, bridge and vehicle dynamics have been shown to be sources of error for Moses' algorithm (O'Brien et al 1999b). Therefore, BWIM systems generally tend to inaccurate for calculating axle weights. Gross vehicle weights are more accurate than axle weights due to the fact that while a long continuous strain record due the whole truck weight is available, it is difficult to distinguish the contributions of each axle. McNulty and O'Brien (2002) reported a field test where inferred gross vehicle weights were within 10% of the statically measured values with a confidence interval of 96.6% and static axle weights were within 15% of the measured values with a confidence interval of 89.3%. Some of the inaccuracies inherent within the Moses algorithm can be improved upon via the tool of regularisation as described in section (2.3). To verify this and to better illustrate the concept of regularisation the method is applied to the original Moses algorithm.

4.3.1 Moses Algorithm

If a vehicle is considered at a certain longitudinal location on a bridge, the gross bending moment at the midspan can be considered as the sum of the individual midspan moments in each girder The bending moment, M_i, in each individual girder is defined by,

$$M_i = E_i Z_i \varepsilon_i \tag{4.15}$$

where Z_i and ε_i are the section modulus and the measured strain at the soffit of the i^{th} girder respectively and E_i is the modulus of elasticity. If it is assumed that the section modulus remains constant for all girders, the total bending moment is given by,

$$M = EZ\sum_{i=1}^{N} \varepsilon_i \tag{4.16}$$

where N is the number of girders. For a truck crossing the bridge with n axles weighing A_1 to A_n, the theoretical midspan strain, ε^{th} at a particular time t can be represented by,

$$\varepsilon^{th}(t_j) = \frac{1}{EZ}\left(I_1(t_j)A_1 + I_2(t_j)A_2 + ... + I_n(t_j)A_n\right) \tag{4.17}$$

where $I_i(t)$ is the influence ordinate of total bending moment at midspan for the i^{th} axle at a particular point in time t_j. Equation (4.17) applies each time the strain is measured as dictated by the scanning frequency of the data acquisition equipment. If the theoretical stain for every point in time considered is written in matrix form, the resulting equations are:

$$\begin{Bmatrix} \varepsilon^{th}(t_1) \\ \varepsilon^{th}(t_2) \\ \varepsilon^{th}(t_3) \\ . \\ . \\ . \\ . \\ \varepsilon^{th}(t_T) \end{Bmatrix} = \frac{1}{EZ}\begin{bmatrix} I_1(t_1) & I_2(t_1) & . & . & I_n(t_1) \\ I_1(t_2) & I_2(t_2) & . & . & I_n(t_2) \\ I_1(t_3) & I_2(t_3) & . & . & I_n(t_3) \\ . & . & & & . \\ . & . & & & . \\ . & . & & & . \\ . & . & & & . \\ I_1(t_T) & I_2(t_T) & . & . & I_n(t_T) \end{bmatrix} \begin{Bmatrix} A_1 \\ A_2 \\ . \\ . \\ A_n \end{Bmatrix} \tag{4.18}$$

where T is the total number of strains calculated. In matrix form this becomes

$$[I_A]\{A\} = \{\varepsilon^{th}\} \tag{4.19}$$

where $[I_A]$ is the matrix of influence ordinates, $\{A\}$ is the vector of axle weights and $\{\varepsilon^{th}\}$ is the vector of theoretical strain. If the vector of theoretical strain is replaced with a vector of measured strain ε^{me}, equation (4.19) is an overdetermined system of equations of the form:

$$[I_A]\{A\} = \{\varepsilon^{me}\} \tag{4.20}$$

The left hand side of equation (4.20) represents the theoretical strain and the right hand side the measured. The objective function to be minimised in the least squares analysis is the sum of the squares of the differences between the theoretical and measured strain:

$$\psi = \sum_{i=1}^{T} (\varepsilon_i^{me} - \varepsilon_i^{th})^2 \tag{4.21}$$

However as the set of equations have already been defined in matrix form the objective function can be defined by,

$$\psi = (\{\varepsilon^{me}\} - [I_A]\{A\})^T (\{\varepsilon^{me}\} - [I_A]\{A\}) \tag{4.22}$$

Expanding equation (4.22) yields an equation of the form,

$$\psi = \{A\}^T [I_A]^T [I_A]\{A\} - 2\{A\}^T [I_A]\{\varepsilon^{me}\} + \{\varepsilon^{me}\}^T \{\varepsilon^{me}\} \tag{4.23}$$

Minimising the objective function ψ with respect to the vector of axle weights results in an equation of the form,

$$([I_A]^T [I_A])\{A\} = [I_A]^T \{A\} \tag{4.24}$$

hence,

$$\{A\} = ([I_A]^T [I_A])^{-1} ([I_A]^T \{\varepsilon^{me}\}) \tag{4.25}$$

4.3.2 Regularised Solution

The solution to the Bridge weigh in motion equations defined by equation (4.25) is what is commonly referred to as the normal equations (Stoer & Burlisch 1992). By adding a regularisation term to equation (4.21) the objective function can be rewritten as:

$$\psi = (\{\varepsilon^{me}\} - [I_A]\{A\})^T (\{\varepsilon^{me}\} - [I_A]\{A\}) + \lambda \{A\}^T \{A\} \tag{4.26}$$

where λ is the non-negative regularisation parameter lying between zero and infinity. Minimising the new objective function with respect to the vector of axle weights yields,

$$[[I_A]^T[I_A]+\lambda I]\{A\}=[I_A]^T\{\varepsilon^{me}\} \tag{4.27}$$

where I is the identity matrix. The solution is now unique to each regularisation parameter and can be defined by:

$$\{A\}_\lambda=([I_A]^T[I_A]+\lambda I)^{-1}[I_A]^T\{\varepsilon^{me}\} \tag{4.28}$$

4.3.3 Results and Analysis

In order to examine the performance of the regularised solution of the Moses equations compared with that of the original equations, a strain signal at the mid-span of the bridge is required. The bridge model outlined in section 4.2 is used, and the state space formulation of the equilibrium equation of motion is used to simulate a truck crossing the bridge. The truck used in all cases is a three axle one with the configuration illustrated in figure 4.4. The truck configuration is chosen arbitrarily, although the axle spacing and static axle loads are thought to be reasonable for a truck of this type.

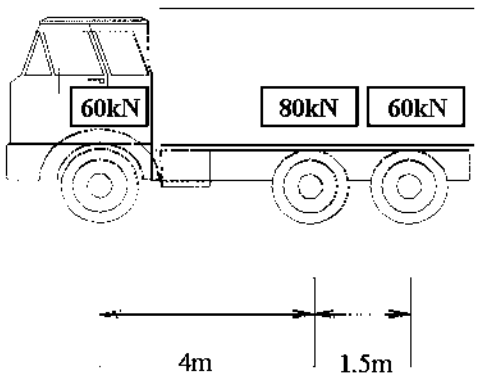

Figure 4.4 – Axle spacing and static axle weights

The algorithm is tested initially for the truck crossing the bridge at 22 m/s with no vehicle dynamics. Hence the truck is treated as three moving constant loads. Figure 4.5a shows the theoretical midspan strain due to the passage of theses forces. In order to accurately assess the sensitivity of the algorithm, it is necessary to introduce a degree of

random error into the theoretical values, as in reality a measured strain signal would contain random measurement error (noise). The theoretical strain signal at the mid span of the bridge is therefore contaminated with two percent Gaussian noise (see figure 4.5b) defined by the equation,

$$\{\varepsilon^{me}\} = \{\varepsilon^{th}\} + P\varepsilon^{th}_{\max}\{N_{oise}\} \tag{4.29}$$

where ε^{th} is the theoretical strain, P is the percentage error, $\varepsilon^{th}_{\max}$ is the maximum theoretical strain induced in the simulation due to the passage of the truck, and N_{oise} is a vector of random numbers with zero mean and standard deviation of one.

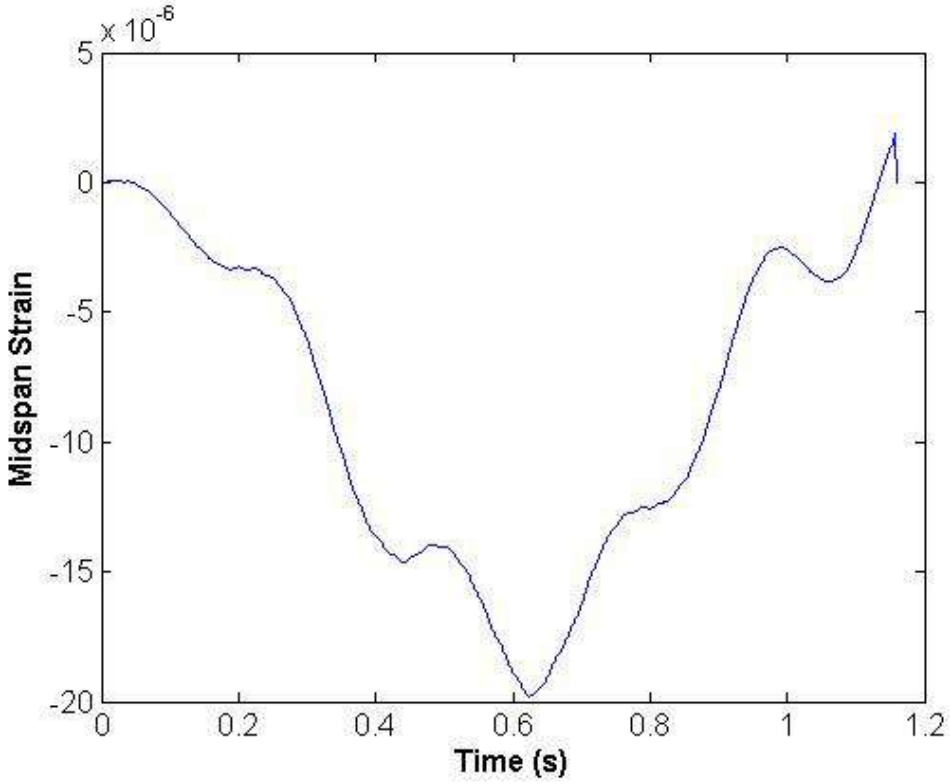

(a) – Theoretical midspan

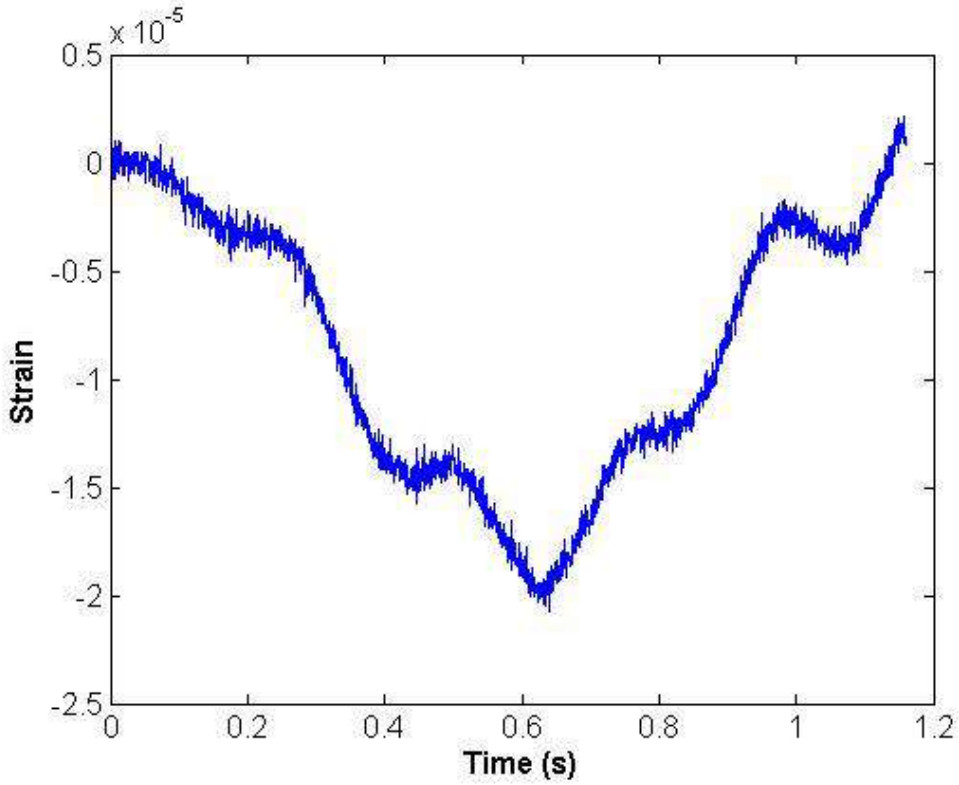

(b) – Noisy Strain signal

Figures 4.5 – Simulated midspan strain due to a three- forces travelling at 22m/s

The final part of the solution to the regularised Moses equations lies in the calculation of the optimal regularisation parameter; again the L-curve has been chosen to obtain the optimum. In the formulation of the Bridge weigh in motion problem as described in section 4.3.2, the residual norm of the error for each specific regularisation parameter λ is defined by,

$$E_{norm} = \sqrt{(\{\varepsilon^{me}\} - \frac{1}{EZ}[I_A]\{A_\lambda\})^T(\{\varepsilon^{me}\} - \frac{1}{EZ}[I_A]\{A_\lambda\})} \qquad (4.30)$$

The norm of the solution for each particular regularisation parameter is defined by,

$$F_{norm} = \sqrt{\{A_\lambda\}^T\{A_\lambda\}} \qquad (4.31)$$

For the truck event described above, the regularisation parameter was varied between 1 $\times$ 10^{-90} and 600,000. Figure 4.6a shows the L-curve over this range of regularisation parameters and figure 4.6b shows approximately where the optimal regularisation parameter lies. A program developed in matlab, was used to calculate the error and solution norms for each value of the regularisation parameter and Hansen's (2001a, 2001b) program plot_lc was used to plot the L-curve. It can be seen from figure 4.6a that the distinctive shape of the L-curve is inherent in the solution and from figure 4.6b the optimal regularisation parameter lies between 90 and 500. Graphically the point of maximum curvature is approximately 200. The axle weights corresponding to each particular regularisation parameter are shown in table 4.2 and the corresponding errors in figure 4.7. A regularisation parameter of zero corresponds to the conventional Moses algorithm. It can be seen that there are significant errors. In particular, there are corresponding errors of about $\pm$ 15% in the two closely spaced axles. The regularised solution represents a significant improvement in the predicted axle weights. For near optimal values of λ, all axle weights are within about 3% of the exact values.

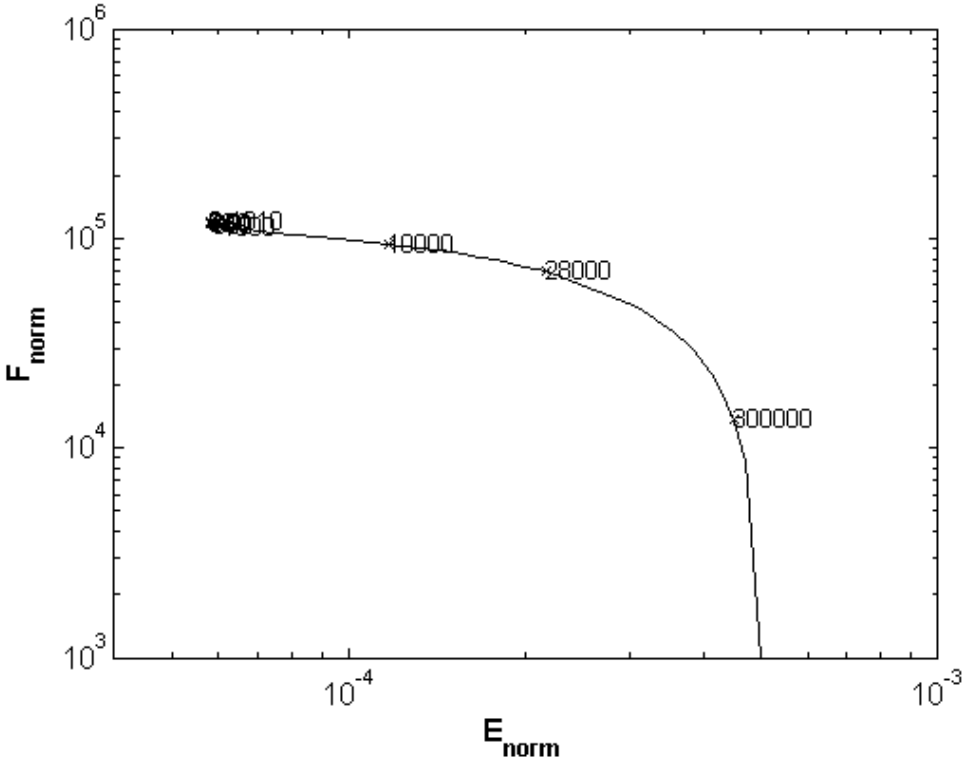

(a) – L-curve

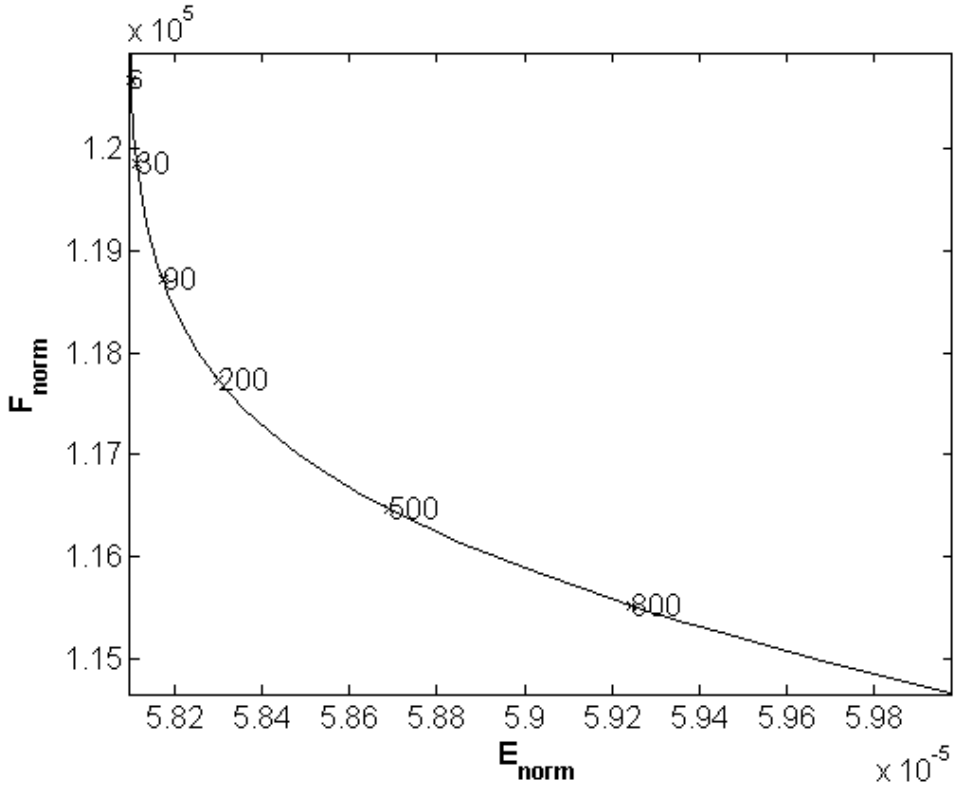

(b) – Optimal range of regularisation parameters

Figures 4.6 – L-curve analysis for the case of constant moving Loads

λ	0	140	180	200	250	300	350	400	Exact
Axle 1 (kN)	56.9	59.6	59.8	60.1	60.3	60.5	60.6	60.7	60
Axle 2 (kN)	93.1	82.4	81.6	80.4	79.2	78.2	77.4	76.8	80
Axle 3 (kN)	52.1	60.1	60.6	61.4	62.2	62.8	63.3	63.6	60

Table 4.2 – Regularised Axle weights corresponding to each particular regularisation parameter

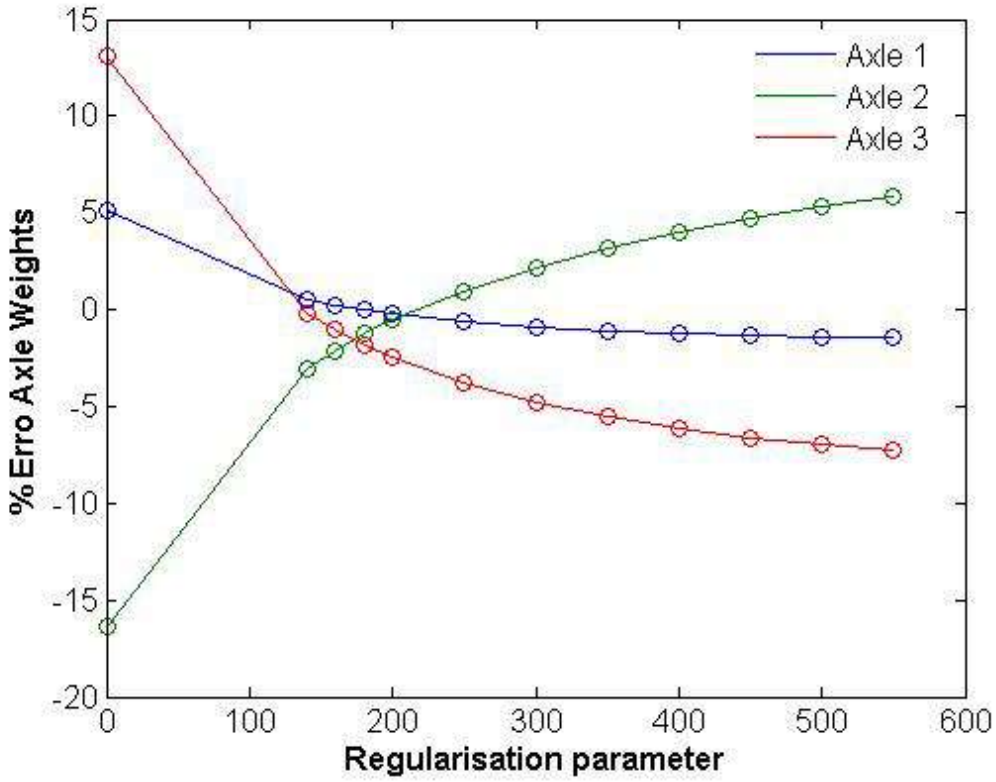

Figure 4.7 – Errors in predicted Axle weights versus the regularisation parameter

It should be noted that the results described above are for the case of zero vehicle dynamics. In order to assess how the algorithm performs under vehicle dynamics, simulations were carried out where each axle contains a time varying component defined by,

$$F_i(t) = A_i(1 + c(\sin(5\pi t)) \tag{4.32}$$

where A_i is the static axle weight for the i^{th} axle and c is the maximum variation to be added to each axle, to represent oscillation in axle force. Initially c was varied from .01 to .05 and it was found that the regularised solution performed equally well for vehicle dynamics less that or equal to 5% see figure 4.8. However it was found that for axle dynamics of 10 or 20% the regularised solution fails to converge see figures 4.9. Nevertheless in all cases the regularised solution offers a significant improvement over that of the conventional algorithm.

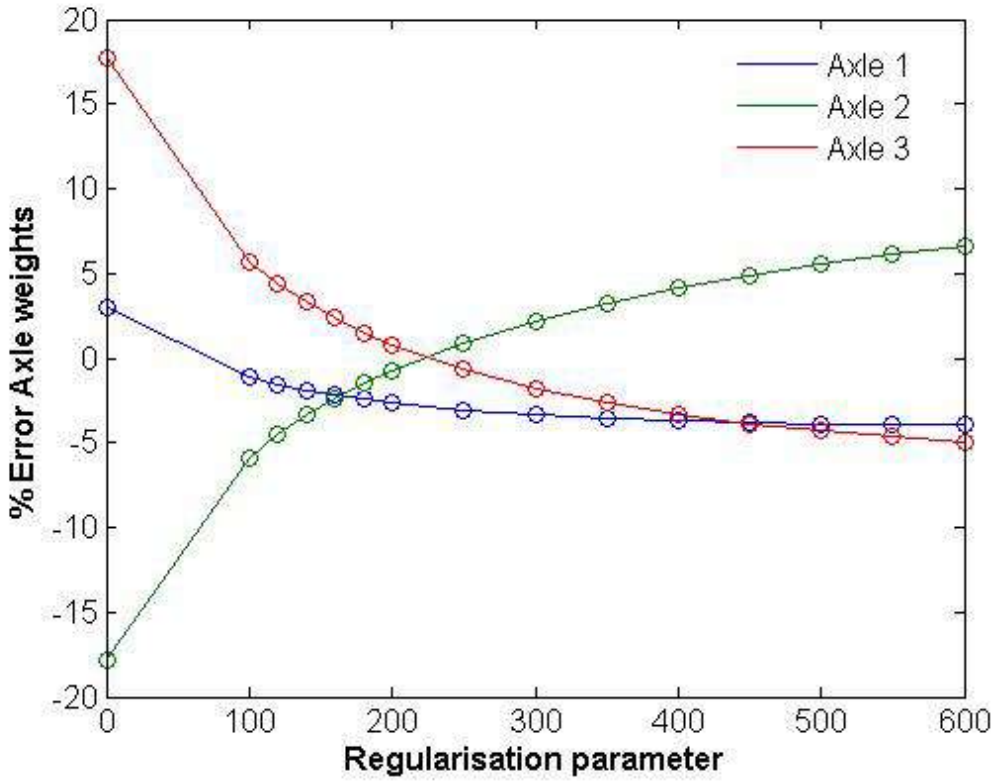

Figure 4.8 – Error in axle weights versus the regularisation parameter for 5% axle dynamics λ is approximately 200.

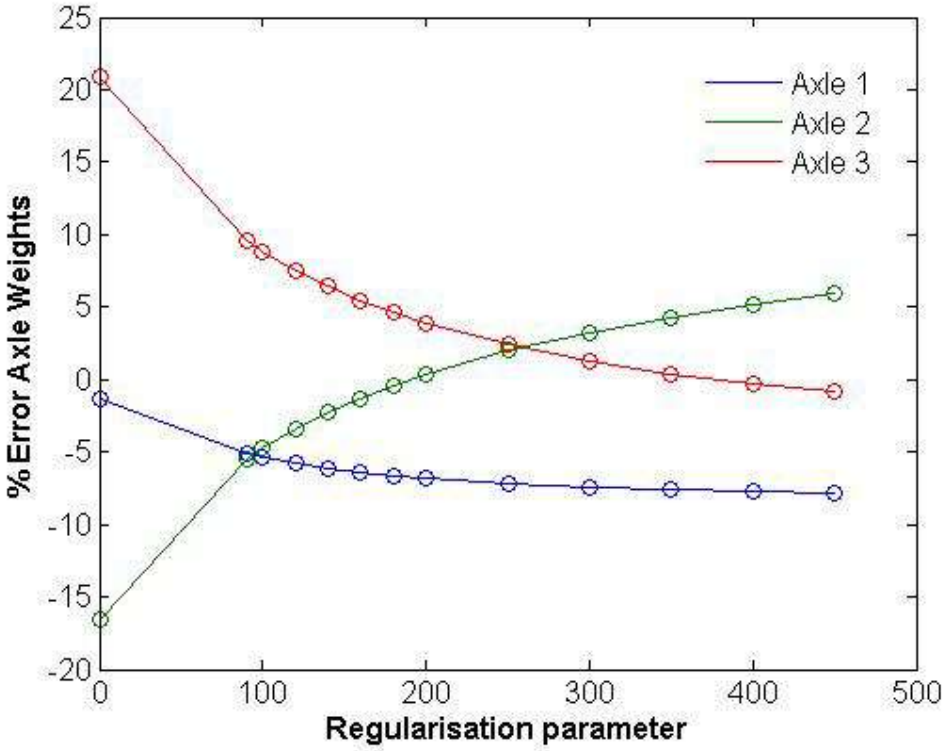

(a) – 10% vehicle dynamics

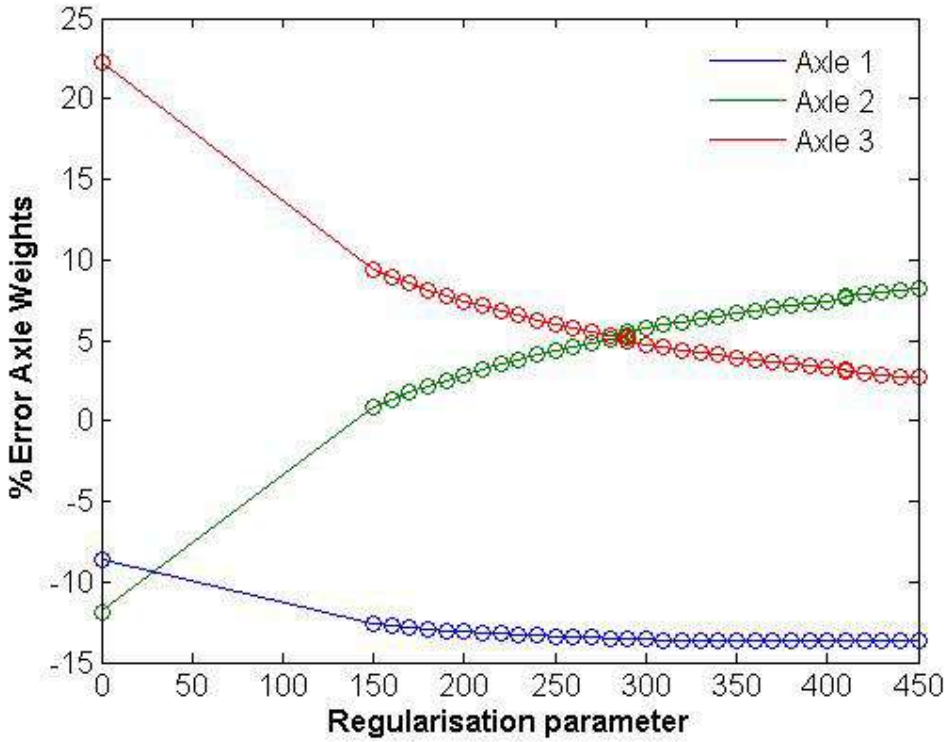

(b) – 20% vehicle dynamics

Figures 4.9 - Error in axle weights versus the regularisation paramater for various vehicle dynamics

4.3.4 Moving Sprung Mass Models

In this section, the bridge response is obtained through convolution of the vehicle loads with modal responses of the bridge. The convolution integral is solved by transformation to the frequency domain using the fast Fourier transform. The method is then extended by an iterative procedure to include dynamic interaction between the bridge and the mathematical model of the vehicle. Green and Cebon (1994) have illustrated the effectiveness of this calculation method, the convergence of the iterative procedure, and have reported good agreement with experimental data.

Through collaboration with Dr. Mark Green, Gonzalez (2001), Gonzalez et al (2002) secured the dynamic bridge responses for heavy vehicles with steel-spring and air-spring suspensions, in order to assess the influence of vehicle suspension on B-WIM systems. The dynamic bridge data provided by Green is used herein to assess the accuracy of the regularised bridge weigh-in-motion (R-B-WIM) algorithm, developed by the author.

The bridge is modelled as a simply supported beam 30m long, with a first natural frequency of 3.33 Hz and 1% damping. Strain output is calculated at midspan every 0.01 s (100 Hz). The Bridge-Weigh-In-Motion (B-WIM) algorithm was calibrated by Gonzalez (2001), i.e., the influence line is found, with a two-axle fully laden linear sprung vehicle (four degrees of freedom). Then, the system is tested with the four-axle vehicle (eleven degrees of freedom) of Figure 4.10 with two different suspension systems representing air and steel leaf. The test vehicle models employed here were developed by Green et al. (1995). In Figure 4.10 elements A, B and C represent non-linear suspension elements, linear springs, and a linear spring/damper combination, respectively. For the vehicle with air suspension, models of air springs with parallel viscous dampers replace the steel-spring elements on the drive axle and the two trailer axles. The suspension on the steer axle is the same for both vehicle models. Two surface profiles, three different speeds (55, 70 and 85 km/h), and two different loading conditions were chosen for the simulations. It should also be noted that the road profiles in both cases contain a bump at 25m, which signficantly affects the imparted wheel forces to the road surface.

The shape of the theoretical influence line is known from beam theory and the static algorithm only requires a calibration factor to adjust the magnitude of the strains to the theoretical model, allowing for *E* and *Z*, which are generally not known in field tests. If the exact influence line for bending moment is used, the calibration factor is the product of the modulus of elasticity and the section modulus (equation 4.15). In the case of an experimental record, there are several approaches that can be used to obtain the real shape of the influence line (O'Brien et al 2006). For this analysis, the calibration factor was obtained by Gonzalez (2001), by dividing the real static gross vehicle weight by the predicted weight of the calibration truck. A linear sprung two-axle vehicle with 4 m axle spacing, 32.42 kN static weight in the front axle and 59.94 kN in the rear axle is used for calibration. The strain record generated by the two-axle vehicle is contaminated with 3% noise according to equation (4.29). The calibration factor changes very slightly with speed and an average value of 2.10×10^{10} is adopted

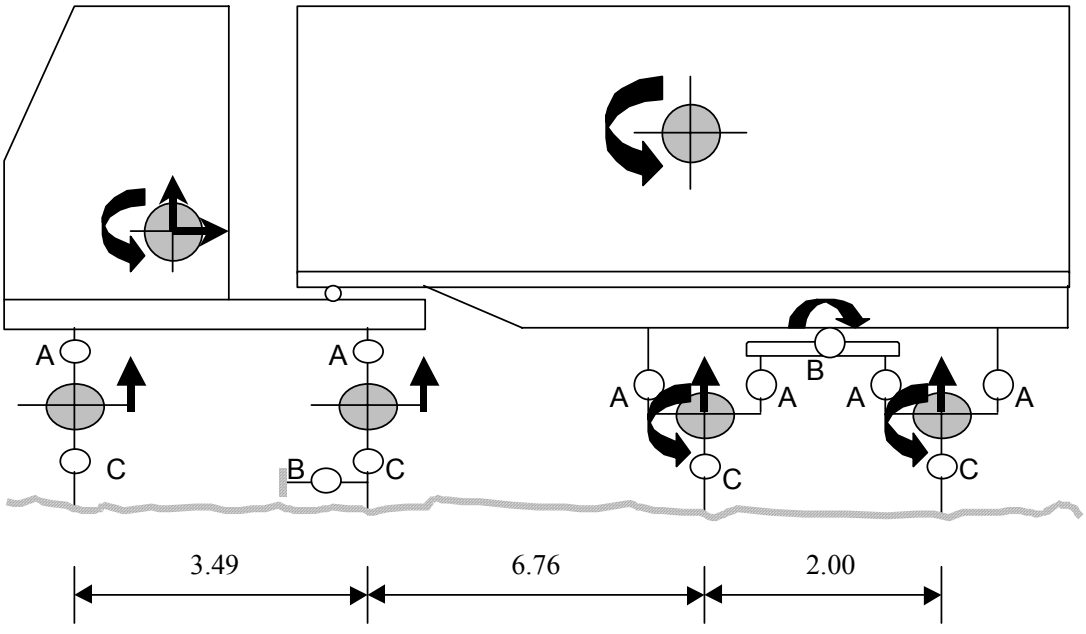

Figure 4.10 – 4-axle vehicle model

Testing with four-axle truck on a smooth profile

The R-BWIM is compared to the conventional B-WIM algorithm using the simulated strain from the Green model on a smooth road profile as defined by the ISO. In total 12 cases are analysed, two loading conditions (fully laden & half laden), three velocities (55, 70 & 80 km/hr) and two types of suspension system (steel sprung & air sprung). The static axle and gross vehicle weights are calculated using the B-WIM and the R-B-WIM, where the optimal regularisation parameter is calculated from the L-curve as defined in section 4.3.3. Figure 4.11 shows the simulated strain due to the passage of two four-axle vehicles at 70 km/h, differentiated by the suspension type only, before being corrupted with noise. As expected, the steel suspension causes higher dynamic oscillations in the strain signal than the air-suspension vehicle.

The % errors in the estimation of the static axle weight by Moses' original algorithm and the new regularised algorithm are given in figures 4.12 and 4.13 respectively. The results found with regularization are generally much more accurate than those found using the original B-WIM algorithm. The improvement is quite significant for axles within a group (3^{rd} and 4^{th} axles) due to the inability of the original B-WIM algorithm to effectively separate weights of closely spaced axles. Table 4.3 summarises the results by both algorithms for the 12 sample runs (2 suspension types, 2 loading conditions and 3 speeds). It can be seen from table 4.3 that the mean error of single axles has been reduced from 20.8% to 5.5% and the mean error of axles within a group has reduced form 50% to 10.6%. In fact for all results the percentage error in axle weights is improved using the regularised solution, however the percentage error in the GVW is slightly disimproved over that of the conventional algorithm.

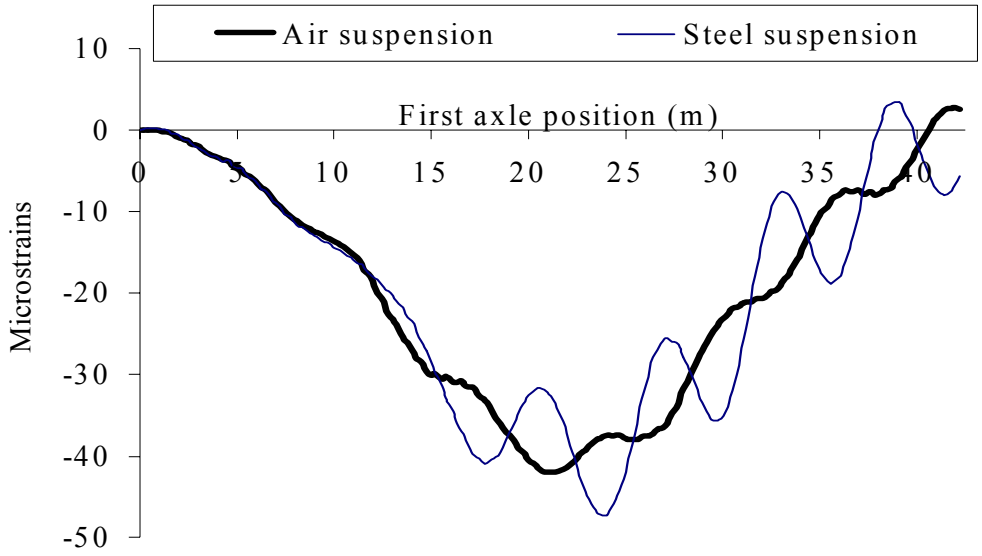

Figure 4.11 - Strain record due to four-axle vehicle travelling at 70 km/h (smooth profile)

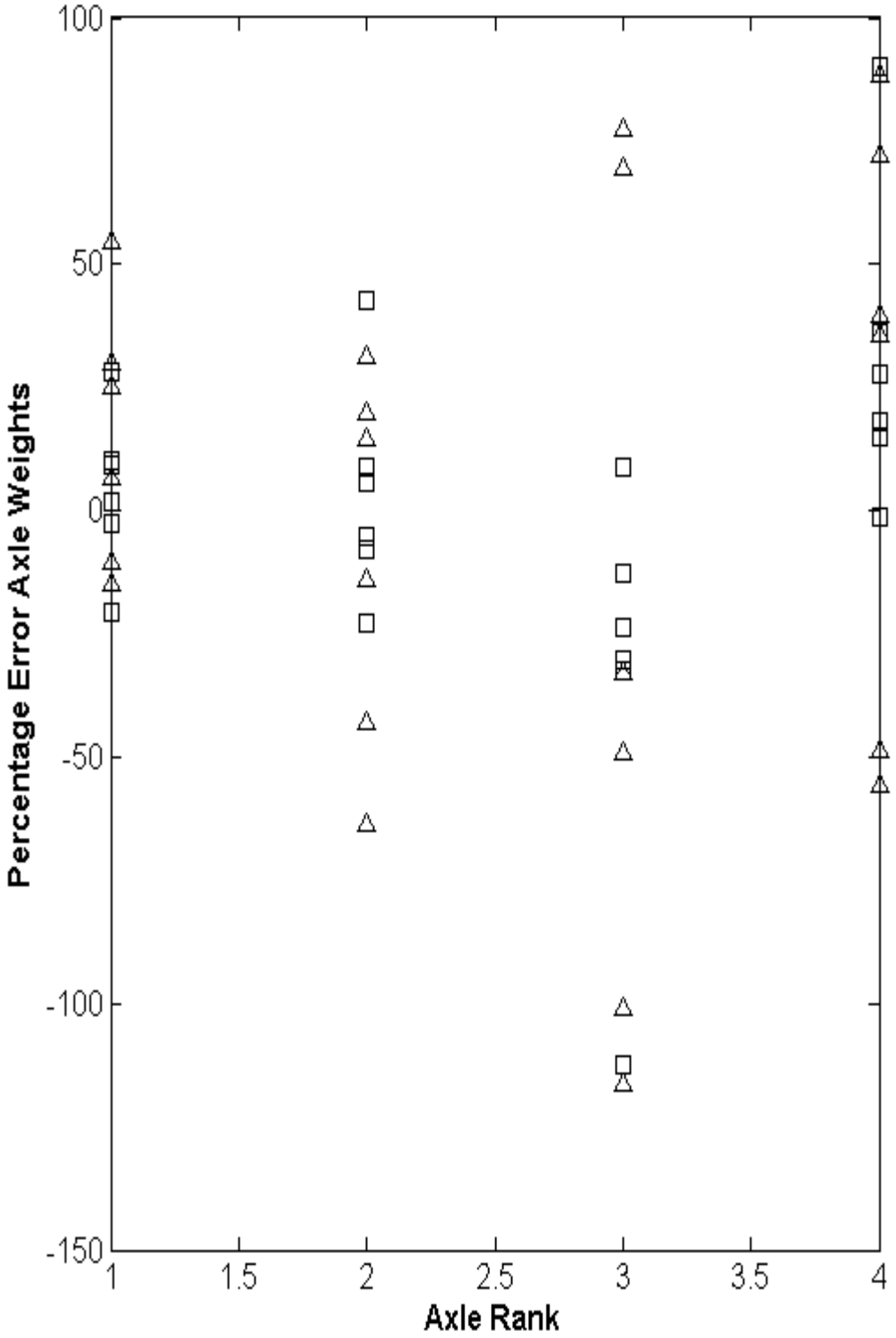

Figure 4.12 - Error versus axle rank for 4-axle truck by conventional B-WIM (smooth profile) (□ air-sprung vehicle, Δ steel sprung vehicle)

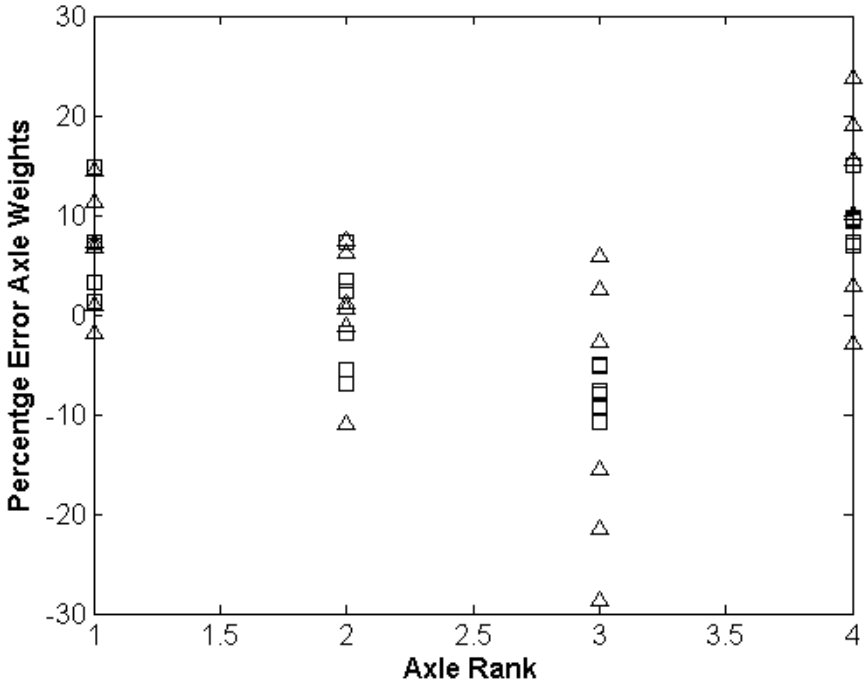

Figure 4.13 - Error versus axle rank for 4-axle truck by regularised B-WIM (smooth profile) (□ air-sprung vehicle, Δ steel sprung vehicle)

		Conventional B-WIM				**Regularised B-WIM**			
Criterion	n	m(%)	s(%)	max(%)	**Class**	m(%)	s(%)	max(%)	**Class**
Single axle (1^{st} & 2^{nd})	24	20.8	16.9	63.5	**E(55)**	5.5	4.2	14.7	**B(10)**
Axle within axle group (3^{rd} & 4^{th})	24	49.8	33.6	116.3	**E(115)**	10.6	7.0	28.6	**D+(20)**
Gross Weight	12	1.0	0.6	2.1	**A(5)**	1.9	1.0	3.7	**A(5)**

Table 4.3 - Relative error statistics by conventional and regularised B-WIM algorithm smooth profile
(n: Total number; m: mean; s: Standard deviation; max: maximum error; class: cost 323 classification)

Testing with four-axle truck on a rough profile

The R-BWIM is compared to the conventional B-WIM algorithm using the simulated strain from the Green model on a rough road profile as defined by the ISO. In total 12 cases are analysed, two loading conditions (fully laden & half laden), three velocities (55, & 80km/hr) and two types of suspension system (steel sprung & air sprung). The static axle and gross vehicle weights are calculated using the B-WIM and the R-B-WIM, where the optimal regularisation parameter is calculated from the L-curve as defined in section 4.3.3. It should be noted that the optimal regularisation parameter has been calculated from the L-curve in all cases, where the criterion that the optimal is the point of maximum curvature, this criterion alone has been used to locate the optimal

On a rough profile, the maximum dynamic response takes place at 70 km/h for the steel-sprung vehicle and it is about three times that obtained on a smooth profile. The maximum dynamic response takes place at 85 km/h for the air-sprung vehicle. The air-suspended vehicle causes significantly lower dynamic bridge response than the steel-spring suspended vehicle and it is less sensitive to a change in speed. These high dynamics suggest the occurrence of frequency matching between the steel-sprung vehicle and the bridge. Consequently, Bridge WIM will tend to be less accurate in the cases of steel-spring suspensions, rough road profiles, and for this bridge, for vehicle speeds near 70 km/h.

For the case of the 4-axle vehicle travelling at 70 km/hr, the conventional Bridge WIM algorithm results in massive errors in the predicted axle weights (-190%, 308%, -645%, 504%; axles 1 to 4 respectively) and relatively small errors in the gross vehicle weight (3.2%). However the regularised B-WIM significantly reduces the errors in the predicted axle weights (-1.7%, 13%, -30%, 30%; axles 1 to 4 respectively) with little or no improvement in the gross vehicle weight (3.1%). The optimal regularisation paramater was calculated from the L-curve to be approximately 350, see figure 4.14.

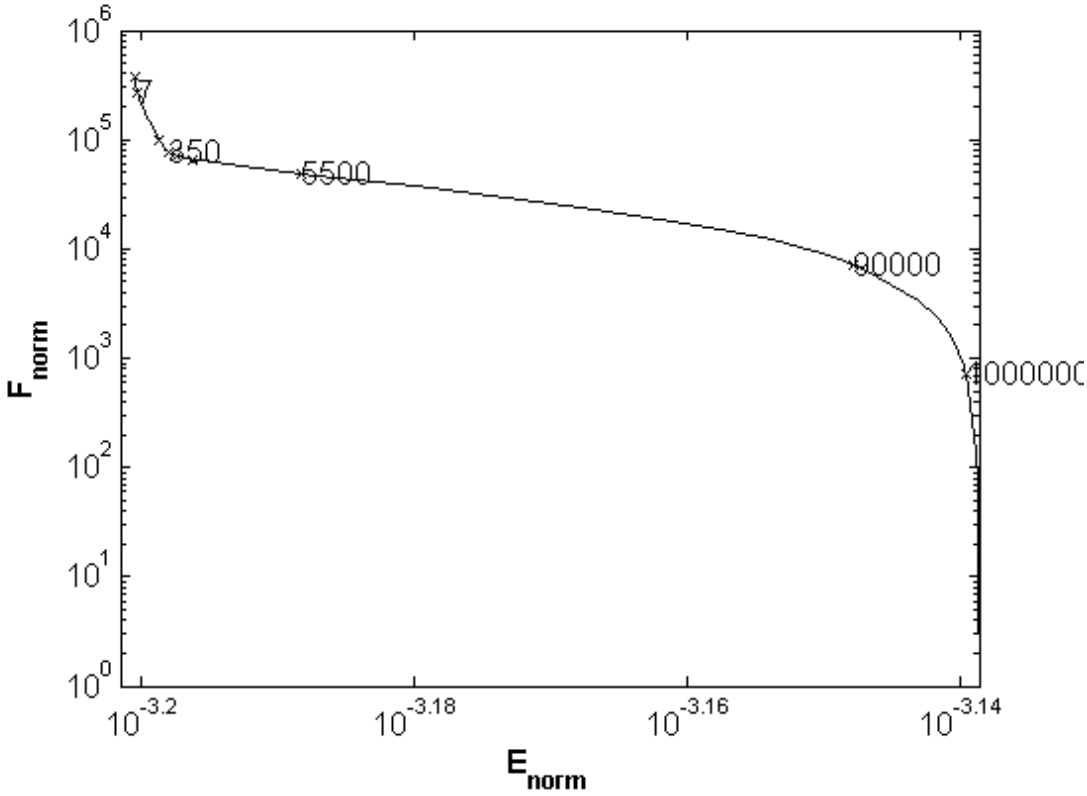

Figure 4.14 – L-curve for four-axle fully loaded vehicle travelling on a rough profile at 70 km/hr with steel suspension system.

It can be seen from figure 4.14 that the distinct shape of the L-curve is clear in this particular solution. Figure 4.15 shows the predicted axle weights for each regularisation parameter. This figure effectively illustrates what it is that regularisation achieves. For very small regularisation parameters where the solution is close to the least squares the predicted axle weights are both positive and negative. However as the regularisation parameter tends towards its optimal value, as predicted by the L-curve, the axle weights are redistributed essentially until the solution converges. As one passes the optimal regularisation parameter the solution diverges again.

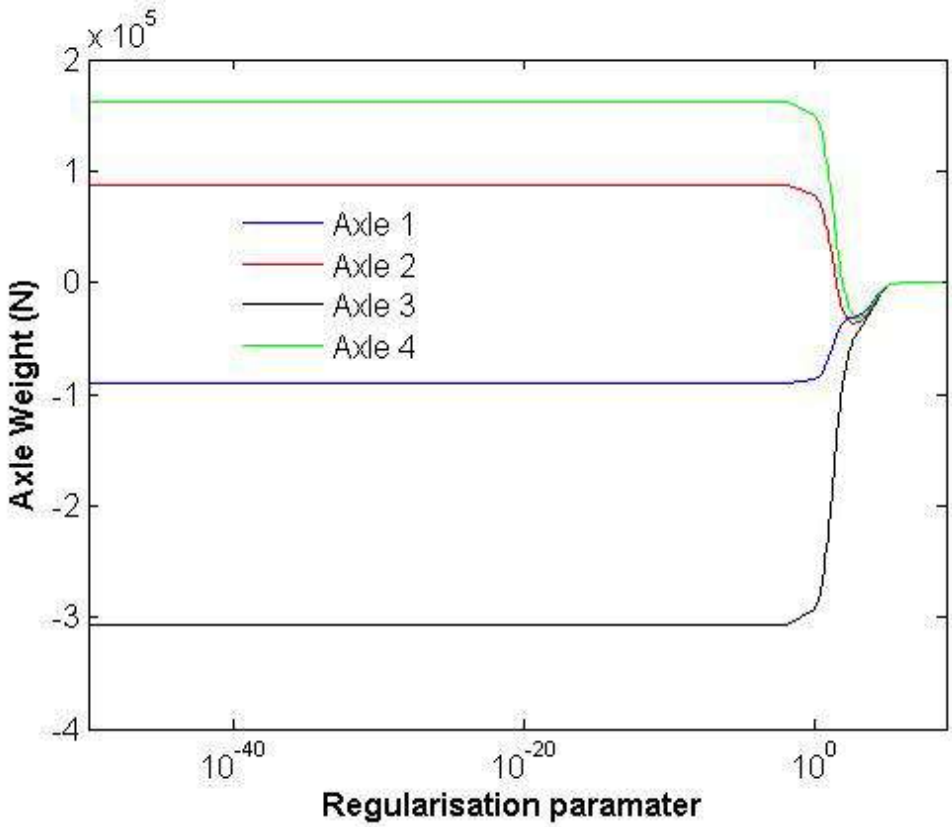

Figure 4.15 – Predicted axle weights versus the regularisation paramater

Figures 4.16 and 4.17 show the % errors in the estimation of static axle weights by both algorithms for all the runs of the four-axle vehicle on a rough profile. The errors in the predictions of static axle weight increased considerably with surface roughness for the B-WIM algorithm (in many cases by over a few 100%). The errors for the regularised B-WIM algorithm have also increased with roughness; they are obviously less sensitive to the dynamic increment in the bridge response than B-WIM. The relative error statistics for both algorithms are presented in Table 4.4.

It can be seen from table 4.4 that the mean error of single axles has been reduced from 117.9% for the conventional B-WIM algorithm to 13.1% for the regularised B-WIM algorithm. The mean error of axles within a group has reduced form 266% to 17.3%. In fact for all results the percentage error in axle weights is improved using the regularised solution. However in contrary to the results obtained on the smooth profile the regularised B-WIM algorithm actually improves the percentage errors in GVW over that of the conventional B-WIM algorithm.

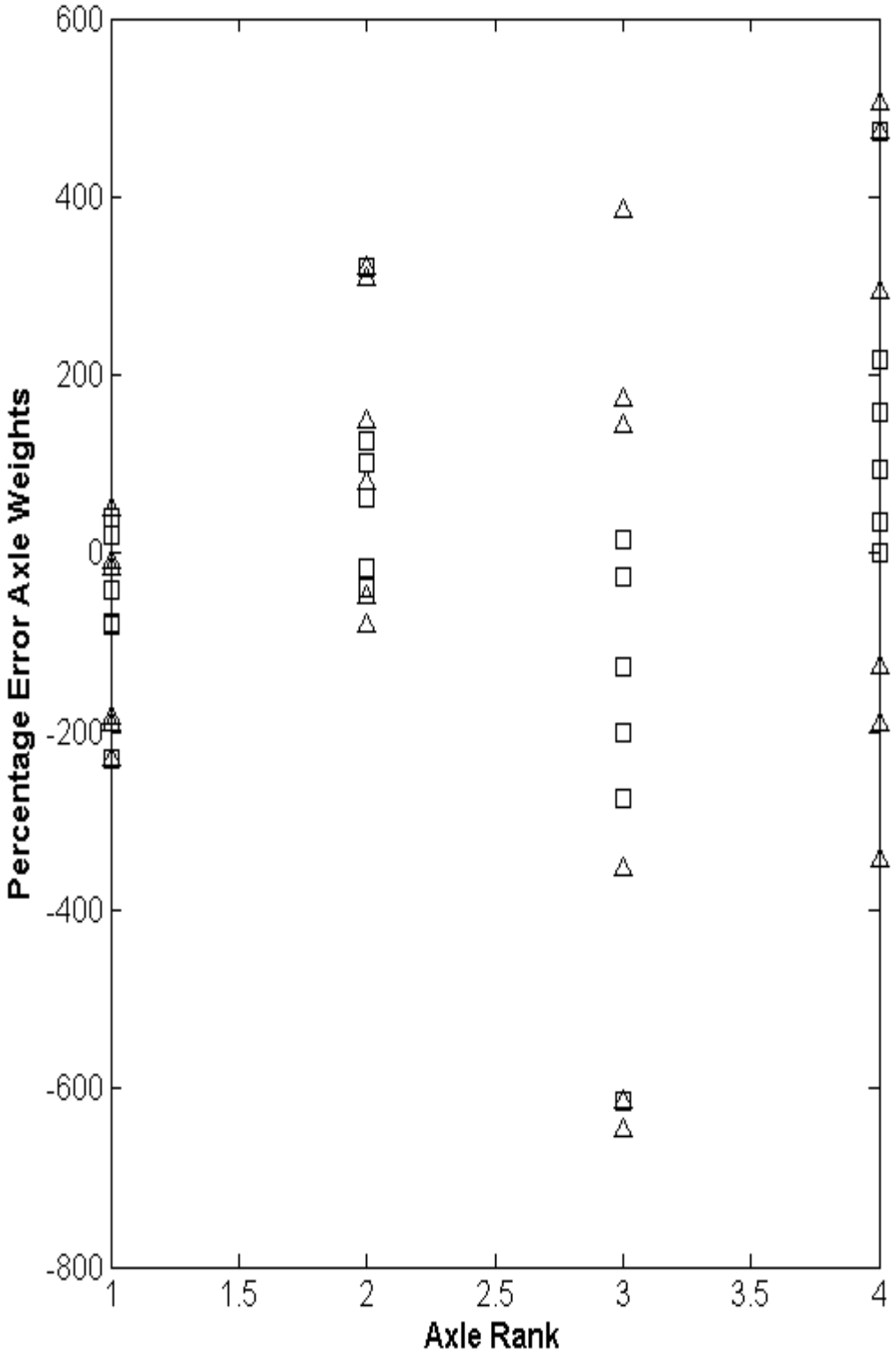

Figure. 4.16 - Error versus axle rank for 4-axle truck by B-WIM (rough profile) (□ air-sprung vehicle, Δ steel sprung vehicle)

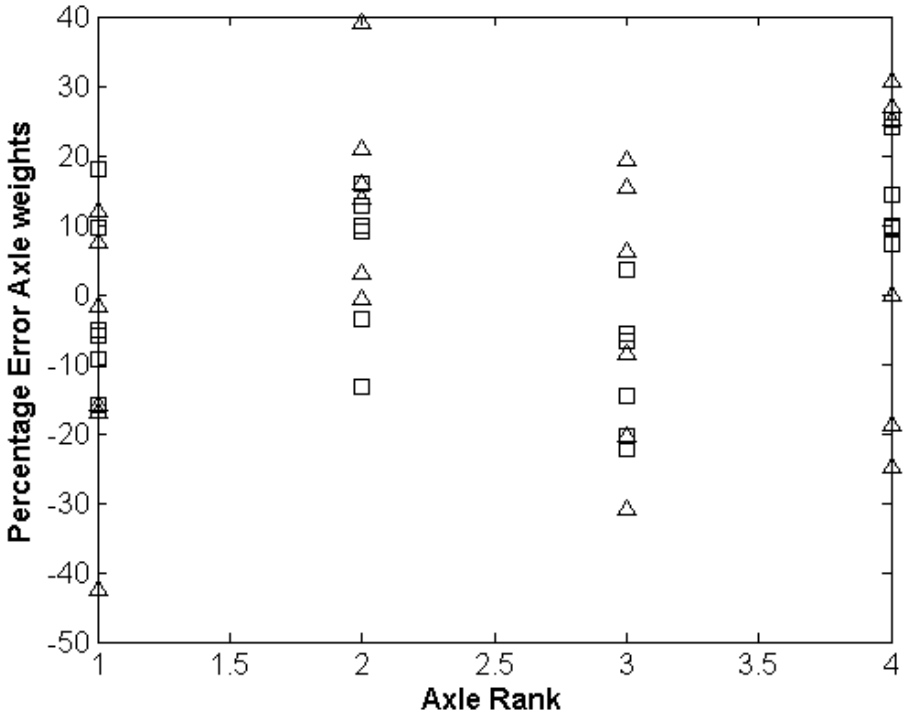

Figure 4.17 -Error versus axle rank for 4-axle truck by RB-WIM (rough profile) (□ air-sprung vehicle, Δ steel sprung vehicle)

		Conventional B-WIM				**Regularised B-WIM**			
Criterion	n	m(%)	s(%)	max(%)	**class**	m(%)	s(%)	max(%)	**class**
Single axle (1^{st} & 2^{nd})	24	117.9	100.8	321.9	**E(330)**	13.1	10.5	42.5	**E(35)**
Axle within axle group (3^{rd} & 4^{th})	24	265.7	208	646	**E(695)**	17.3	8.8	30.8	**E(30)**
Gross Weight	12	3.4	3.8	12.2	**C(15)**	2.5	2.1	8.2	**B+(7)**

Table 4.4. Relative error statistics by conventional and regularised B-WIM algorithm rough profile
(n: Total number; m: mean; s: Standard deviation; max: maximum error; class: cost 323 classification)

4.4 Conclusions

Moses algorithm remains as the basis for commercial B-WIM systems. One of its main advantages is its relatively good accuracy, in particular for gross vehicle weights, and the ease of implementation compared to other theoretical developments requiring complex dynamic models and abundant instrumentation. This chapter has presented an improvement in accuracy over Moses original algorithm without increasing the needs for the B-WIM installation and calibration. The new B-WIM algorithm employs the method of Tkhonov regularisation in conjunction with the Moses equations to derive a new better-conditioned formulation of the B-WIM equations.

The conventional B-WIM and regularised B-WIM are initially tested using the simulated strain from a finite element model subject to moving constant and time varying forces. This method of simulation using the finite element method is used throughout this thesis for the numerical testing of other inverse methods.

The method is theoretically tested using dynamic simulations of a series of moving forces on a bridge; it has been shown that, for relatively low vehicle dynamics less than 10%, the new algorithm significantly improves the errors in predicted forces using the conventional B-WIM. However for vehicle dynamics greater than or equal to 10% the convergence of the regularised B-WIM equations are not as acute. Nevertheless there is still a significant improvement over that of the conventional B-WIM equations alone.

Further to this, through a collaborative study between Gonzalez (2001) and Green, dynamic simulations from a complex vehicle bridge interaction model were made available to test the algorithm. From the results of this analysis it can be concluded that in all cases the regularised B-WIM algorithm out performs that of the conventional algorithm in terms of the calculated axle weights. What is particularly advantageous of this approach is its relative ease of implementation and its compatibility with existing commercial B-WIM systems. Whereby no additional instrumentation is necessary and calibration factors would be identical to those originally identified in the field.